Available online at www.sciencedirect.com

ScienceDirect

Geochimica et Cosmochimica Acta 71 (2007) 3872–3886

Geochimica et Cosmochimica Acta

www.elsevier.com/locate/gca

Redox evolution and mass transfer during serpentinization: An experimental and theoretical study at 200 °C, 500 bar with implications for ultramafic-hosted hydrothermal systems at Mid-Ocean Ridges

W.E. Seyfried Jr. *, D.I. Foustoukos [1], Qi Fu

Department of Geology and Geophysics, University of Minnesota, Minneapolis, MN 55455, USA

Received 11 December 2006; accepted in revised form 21 May 2007; available online 2 June 2007

Abstract

Highly reducing and high-pH vent fluids characterize moderately low temperature ultramafic-hosted hydrothermal systems, such as the recently discovered Lost City hydrothermal field at 30°N Mid-Atlantic Ridge Ridge (MAR). To better understand the role of mineral reaction rates on changes in fluid chemistry and mineralization processes in these and similar systems, we conducted an experimental study involving seawater and peridotite at 200 °C, 500 bar. Time series changes in fluid chemistry were monitored and compared with analogous data predicted using experimental and theoretical data for mineral dissolution rates. Although there was qualitative agreement between predicted and measured changes in the chemical evolution of the fluid for some species, the rate and magnitude of increase in pH, dissolved chloride and H_2 did not agree well with predictions based on theoretical modeling results. Experimental data indicate that dissolved H_2 abruptly and intermittently increased, reaching a value only approximately 20% of that predicted assuming magnetite as the primary Fe-bearing alteration phase. The distribution and valence of Fe in primary and secondary minerals reveal that the most abundant secondary mineral, serpentine, contained significant amounts of both ferric and ferrous Fe, with the less abundant brucite, also being Fe-rich ($X_{Fe} = 0.3$). Surprisingly, magnetite was present in only trace amounts, indicating that H_2 generation was largely accommodated by the formation of Fe–chrysotile. Accordingly, the diversity of Fe-bearing secondary minerals together with rates of serpentinization less than theoretically predicted, account best for the relatively low dissolved H_2 concentrations produced. Thus, the experimental data can be used to obtain provisional estimates of thermodynamic data for Fe-bearing minerals, enhancing the application of reaction path models depicting mass transfer processes during serpentinization at mid-ocean ridges. Similarly, the observed differences between theoretically predicted and experimentally measured pH values result from constraints imposed by complex patterns of mass transfer inherent to the experimental system. In particular, the experimental observation of a late stage increase in Na/Cl ratio likely results from the dissolution of a Na_2O component of clinopyroxene, which causes pH to increase sufficiently to induce precipitation of a Ca-bearing phase, perhaps portlandite. As with the redox variability observed during the experiment, this event could not be predicted, underscoring the need to use caution when modeling alteration processes in the chemically complex ultramafic-hosted hydrothermal systems at elevated temperatures and pressures.

1. INTRODUCTION

It is now well recognized that tectonic forces associated with slow spreading mid-ocean ridges result in exposure of mantle-derived ultramafic rocks, especially at ridge/

---

* Corresponding author.
E-mail address: wes@umn.edu (W.E. Seyfried).

[1] Present address: Geophysical Laboratory, Carnegie Institution of Washington, 5251 Broad Branch Road, NW, Washington, DC 20015, USA.

0016-7037/$ - see front matter © 2007 Elsevier Ltd. All rights reserved.
doi:10.1016/j.gca.2007.05.015

transform intersections where extensive crustal thinning and formation of long-lived low angle faults exist (Cannat et al., 1992; Cannat, 1993; Escartin et al., 1997; Escartin and Cannat, 1999). The consequences of this are important for a wide range of geophysical and geologic processes, including crustal rheology and magnetization (Oufi et al., 2002), the cycling of elements between seawater and exposed ultramafic rocks (Janecky, 1986; Allen and Seyfried, 2003; Bach et al., 2004), and the more recently recognized linkage between serpentinization and microbial processes (Alt and Shanks, 1998; Kelley et al., 2001, 2005; Oufi et al., 2002; Allen and Seyfried, 2003; Bach et al., 2004; Schrenk et al., 2004).

Although mineralogical changes associated with subseafloor serpentinization of ultramafic rocks at mid-ocean ridges are well understood, mass transfer processes with reaction progress are less clear. Bach et al. (2006) recently reported results of detailed petrographic and mineral chemical studies of serpentinites from 15°N Mid-Atlantic Ridge (MAR) (ODP Leg 209), which carefully and effectively linked mineral chemistry and rock texture with the sequence of serpentinization reactions. Accordingly, this study showed that early stage serpentinization reactions likely occur at low-fluid flux giving rise to near-isochemical alteration of olivine to serpentine and ferroan brucite. Subsequent reactions reveal the effects of greater amounts of fluid flow resulting in the breakdown of ferroan brucite. This stage in the paragenesis may be linked to pyroxene-derived sources of dissolved silica and the increasing ineffectiveness of olivine to constrain pH and buffer redox (Allen and Seyfried, 2003). Indeed, an important observation stemming from the ODP Leg 209 geochemical, textural and mineralogical data (Bach et al., 2006), is the relative lack of magnetite during incipient stages of serpentinization, consistent with Fe-enrichment in serpentine and brucite. This alteration stage is then followed by extensive magnetite formation, corresponding with a predictable decrease in fluid pH. Late stage formation of magnetite in oceanic serpentinites described above is generally in keeping with patterns in rock density and rock magnetic properties recognized by others (Toft et al., 1990; Oufi et al., 2002).

The model advanced by Bach et al. (2006) necessarily involves time series variability in the magnitude and rate of production of dissolved hydrogen. Considering the importance of dissolved H_2 as a constraint on mineralization and microbial processes (Schrenk et al., 2004), it is important to examine this further. Thus, here we describe results of an experiment simulating subseafloor serpentinization reactions at 200 °C, 500 bar, while time series changes in dissolved hydrogen were explicitly monitored along with other components that can be linked to the sequence of mineral alteration processes. Moreover, owing to advances in theoretical geochemistry, the experimental data can be directly compared with rates of mineral dissolution and precipitation reactions predicted from mineral kinetic data, which may help to distinguish cause and effect relations observed with reaction progress. The experimental and theoretical data from this study can be applied to interpret better subseafloor alteration processes in ultramafic-hosted hydrothermal systems, provided temperature and pressure conditions are similar to those emphasized here. Results of the study may also find application to processes contributing to the compositional evolution of fluids issuing from seamounts overlying the subducting Pacific Plate, where serpentinization reactions are indicated (Mottl et al., 2004).

2. EXPERIMENTAL, ANALYTICAL AND THEORETICAL METHODS

Peridotite composed of 62 vol % olivine, 26 vol % orthopyroxene, 10 vol % clinopyroxene and ~2 vol % spinel (Table 1) was used for the experiment and is described in greater detail by Zimmerman and Kohlstedt (2004). Based on bulk composition, the peridotite can be more strictly defined as spinel lherzolite, which is an important component of oceanic mantle rock exposed on the seafloor (Snow and Dick, 1995). The peridotite sample was disaggregated, ground with an agate mortar and pestle, and subsequently dry sieved to retain the fraction between 50 and 100 μm in size.

Table 1
Composition of primary minerals in peridotite (lherzolite[a]) determined by electron microprobe (individual minerals) and ICP-MS (bulk rock)

Component	Orthopyroxene	Olivine	Clinopyroxene	Bulk rock
SiO_2	54.89	41.00	52.74	44.99
TiO_2	0.04	0.00	0.37	0.06
Al_2O_3	4.03	0.01	5.82	2.23
Cr_2O_3	0.38	0.00	0.86	nd
FeO	5.60	9.19	2.62	8.72
MnO	0.09	0.12	0.10	0.13
MgO	33.86	49.75	16.15	41.36
CaO	0.66	0.08	19.04	2.06
Na_2O	0.10	0.00	1.55	0.27
K_2O	0.02	0.01	0.02	0.16
H_2O	nd	nd	nd	nd
Total	99.67	100.16	99.28	100.06

	Atoms		
	6 (O) Basis	4 (O) Basis	6 (O) Basis
Si	1.90	1.00	1.91
Ti	0.00	0.00	0.01
Al	0.16	0.00	0.25
Cr	0.01	0.00	0.02
Fe^{2+}	0.16	0.19	0.08
Mn	0.00	0.00	0.00
Mg	1.75	1.81	0.87
Ca	0.02	0.00	0.74
Na	0.01	0.00	0.11
K	0.00	0.00	0.00
Atomic ratios (%)			
Mg	91.50	90.50	51.40
Fe	8.50	9.50	4.70
Ca			43.70

nd, not determined.

[a] Zimmerman and Kohlstedt (2004).

Artificial seawater was prepared with analytical-grade chloride, sulfate and bicarbonate salts from Alfa-Aesar and deionized water to match exactly the dissolved major element chemistry of natural seawater.

The peridotite (40 g) and artificial seawater solution (44 g) were combined and loaded into a flexible Au/Ti reaction cell, which in turn was placed in a steel-alloy autoclave, following procedures described in Seyfried et al. (1987). The flexible gold reaction cell allows on-line sampling of the aqueous fluid at constant temperature and pressure simply by adding water under pressure to the autoclave surrounding the cell. Thus, internally filtered fluid samples can be obtained from the reaction cell contents at any time during an on-going experiment.

Fluid samples from the experiment were analyzed for dissolved components by inductively-coupled plasma mass spectrometry (ICP-MS) (cations), ion chromatography (IC) (anions), while dissolved hydrogen was determined with a Perkin-Elmer Auto-system gas chromatograph (GC), making use of a 30-m, 0.53-mm (ID) fused silica capillary column (Carboxen 1010 PLOT) (Supelco) and thermal conductivity detector (TCD). Dissolved H_2S was determined with a 2-step precipitation–oxidation process, following methodologies described in Foustoukos and Seyfried (2005). The pH of fluid samples was determined using a Ross micro combination electrode at 25 °C with an uncertainty estimated to be approximately ±0.1 units of the reported value. Replicate measurements of all other components of fluid samples indicate analytical precision to be within ±2–5% depending on concentration (Table 2).

A variety of microscopic and analytical techniques were used to characterize solid reactants and experimental run products, including X-ray diffraction (XRD), Electron Microprobe Analysis (EMPA) and Scanning Electron Microscopy (SEM). Powder X-ray diffraction (XRD) analysis was carried out using a Rigaku Multi-flex system equipped with a Cu anode operated at 45 kV and 40 mA and a divergent beam monochromator.

The chemical composition of peridotite-bearing minerals before and after hydrothermal alteration was determined with a JEOL JXA-8900 microprobe. The JXA-8900 also provided integrated high-resolution SEM and WD/ED capabilities, facilitating mineral identification and quantitative analysis. Operation accelerating voltage was 15 kV, while beam current and size were 15 nA and ~1 μm, respectively. The equipped Energy Dispersive X-ray Spectrometer (EDS) system has an EDAX thin window and CDU LEAP detector. The low energy X-ray detection with FEG provided high spatial resolution for microanalysis down to ~0.1 μm^3 under operational conditions.

In addition to detailed chemical and mineralogical examination of minerals, serpentine, which represented the dominant secondary phase, was analyzed using Mössbauer spectra with a conventional constant-acceleration spectrometer (Ranger). This instrument was used in transmission geometry with a $^{57}Co/Rh$ source and α-Fe at room temperature to calibrate isomer shifts and velocity scale. In addition, to better quantify the extent of magnetite formation during the experiment, saturation magnetization of the bulk alteration products was determined. This was accomplished by room temperature hysteresis loop measurements using a Princeton Measurements Corporation vibrating sample magnetometer (VSM). All Fe-valence and magnetic measurements of secondary minerals from the experiment were determined at the Institute for Rock Magnetism, University of Minnesota.

Distribution of aqueous species calculations were made for all fluid samples taking account of mass balance, mass action and charge balance constraints, together with constrains imposed by the revised HKF equation of state (Shock and Helgeson, 1988, 1990; Tanger and Helgeson, 1988; Johnson et al., 1992). In practice, calculations of ion activities of dissolved species and mineral saturation states were modeled using GWB and EQ3/6 software packages (Wolery and Daveler, 1992; Bethke, 1994). The default database for these codes, however, was replaced by another, which was generated for 200 °C, 500 bar using SUPCRT92 (Johnson et al., 1992), and the 1998 database update (Shock et al., 1997; Sverjensky et al., 1997).

Dissolution kinetics of principal silicate minerals in the peridotite were also modeled with GWB and EQ3/6 software packages at 200 °C, 500 bar as a means of comparison with the time series experimental data, using the following generalized rate law:

$$r = \pm k \cdot S \cdot [(1 - \exp(\Delta G_r/RT))] \quad (1)$$

Table 2
Summary of methodology and analytical precision for determination of the composition of aqueous fluids and minerals measured during the experimental study (see text)

Species/component	Methodology	Precision (2σ)
Cl, SO_4	Ion chromatography	2%
Na, K, Mg, Ca, Fe, $SiO_{2(aq)}$	Inductively-coupled plasma mass spectrometry	2% for major species, 5% for minor species and dissolved silica
H_2	Gas chromatography—TCD	10%
pH	Ross micro combination electrode at 25 °C	0.1 units of the recorded value
$H_2S_{(aq)}$	$CuCl_2$-precipitation/H_2O_2 reduction	10%
Major elements in lherzolite and mineral separates	EOL JXA-8900 microprobe	~2%
Major elements in rock	ICP-MS following acid digestion	2%
Ferric/ferrous Fe in serpentine	Ranger Mössbauer spectrometer	
Magnetite	Vibrating sample magnetometer	Sensitivity: 2E−8 A m^2

Table 3
Data[a] used to calculate mineral dissolution rate constants at experimental conditions

Minerals	Activation energy (kJ/mol)	Log dissolution rate[b] (Log mol/cm^2 s)	Sources
Forsterite	37.8	−14.21	Murphy and Helgeson (1987); Pokrovsky and Schott (2000)
Diopside	40.6	−14.79	Knauss et al. (1993)
Enstatite	49.0	−14.75	Schott et al. (1981)

[a] The parameters for kinetic modeling at 200 °C were derived from the Arrhenius equation.

[b] Dissolution rates were determined from silica release rates in experiments at 25 °C (22 °C for enstatite) at near neutral conditions (see text).

where r is the rate of dissolution (−)/precipitation (+) reaction (mol s^{-1}), ΔG_r is the Gibbs free energy of the reaction under the conditions of interest, k is the rate constant for the reaction, S is the surface area (cm^2), R is the gas constant, and T is temperature in Kelvin. The dissolution rate constants for forsterite, enstatite and diopside at experimental conditions were estimated from experimental data at 25 °C for near neutral conditions (Schott et al., 1981; Murphy and Helgeson, 1987; Knauss et al., 1993; Pokrovsky and Schott, 2000), together with activation energy data (Table 3) and constrains imposed by the Arrhenius equation. It was further assumed that the fayalite and ferrosilite components of olivine and orthopyroxene solid solutions dissolved at rates similar to forsterite and enstatite, respectively, possibly introducing limitations in the accuracy of theoretical estimations. Surface area of individual minerals was estimated from constraints imposed by average grain size and shape consistent with crystallographic considerations. In effect, the rate equation is analogous to that developed previously from transition state theory for heterogeneous mineral dissolution at constant temperature and pressure conditions (Lasaga, 1981). The functionality of the bracketed term in (1), however, indicates that for conditions far from equilibrium, the dissolution reaction rate will be independent of Gibbs free energy of reaction, (ΔG_r). As equilibrium is approached, however, ΔG_r becomes increasingly important in accounting for rate data (Lasaga, 1981; Aagaard and Helgeson, 1982; Helgeson et al., 1984; Murphy and Helgeson, 1987; Nagy, 1995). Considering the relative stability of peridotite-bearing minerals (e.g., olivine, orthopyroxene, clinopyroxene) at the conditions of the experiment, it is likely all minerals, with the possible exception of the diopside component of cpx, remain sufficiently far from equilibrium so as to preclude near equilibrium effects slowing reaction progress.

3. RESULTS

3.1. Fluid chemistry

As anticipated from constraints imposed by the relative abundance of fluid and solid (lherzolite) (∼1:1) used for the experiment, dissolved Na, K and Cl concentrations increased with reaction progress, since these species typically are conservative during hydration and hydrolysis of minerals in the ultramafic system, especially at low to moderate temperatures and pressures (Seyfried and Dibble, 1980; Janecky and Seyfried, 1986). The dissolved concentrations of these species do not increase smoothly with time, but rather show a series of plateaus before increasing more noticeably towards the end of the experiment, although this is less the case for dissolved Na and K (Table 4).

Dissolved alkaline earth elements, in contrast, tend to decrease with reaction progress (Table 4 and Fig. 1). Considering the bulk composition of the system, fluid/rock mass ratio, together with temperature and pressure effects, the decrease in Mg is not surprising (Janecky and Seyfried, 1986). What is surprising, however, is the decrease in dissolved Ca, which takes place after approximately 700 h of reaction. A number of other changes occur at this time in the experiment, suggesting a coupled relationship. In particular, it is at or after this time that there is a notable increase

Table 4
Changes in the concentration (mm/kg[a]) of dissolved species in aqueous fluid coexisting with peridotite (lherzolite) and its alteration products with reaction progress at 200 °C and 500 bar

Time (h)	$pH_{(25\,°C)}$	H_2	Cl	H_2S	SO_4	Na	K	Mg	Ca	Si	Fe
0	6.2	0	536	0	32	466	9.0	59	12	0	0
75	6.2	0	542	0	4.5	478	10.7	7.0	24	0.43	0.19
694	nd	0.19	541	0.06	1.7	472	10.5	2.0	30	0.29	0.2
2209	9.7	25.6	528	0	5	511	10.4	0.02	7	0	0.02
3050	11.4	58.3	557	0	6.7	562	11.0	0	6	0	0.08
3705	12.1	57.4	563	0	6.6	603	15.8	0	6	0	0
5187	12.1	76.4	590	0	6.6	588	14.3	0	7	0	0
7875	12.2	76.7	597	0	5.3	593	14.0	0	8	0	0

pH refers to the value measured at 25 °C following sample processing.

nd, stands for species not measured at a given time interval.

[a] mm/kg units refer to mmol per kg solution.

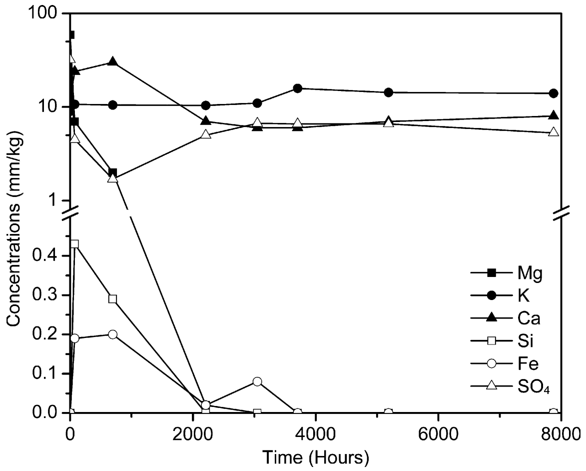

Fig. 1. Measured concentrations of dissolved species (Mg, K, Ca, Si, Fe, and SO_4) in aqueous fluid coexisting with peridotite and its alteration products as a function of time at 200 °C and 500 bar.

in pH (measured at 25 °C) (Table 4). For example, as the pH increased to 9.7 dissolved Ca decreased to 7 mm/kg, but generally maintained this concentration throughout the remainder of the experiment, suggesting mineral buffering effects. Perhaps the most conspicuous aspect of the experiment, however, is the sharp increase in $pH_{(25\ °C)}$ to 12.1 approximately mid-way through the experiment, a value that remained little changed subsequently. This high pH no doubt requires enhanced cation solubility as well to balance charge, although the mechanism by which this was achieved is not clear from absolute cation concentrations shown in Table 4. In any event, the pH increase clearly imposed a key constraint on fluid–mineral equilibria, as suggested by the quantitative decrease in dissolved silica and Fe, as well as, the previously mentioned changes in dissolved Ca (Table 4 and Fig. 1).

In a manner opposite to the pattern displayed by dissolved Ca with reaction progress, dissolved sulfate decreased then increased to a steady state value, suggesting solubility control, possibly by anhydrite.

Dissolved hydrogen increased throughout the experiment, although as with many other species it did so intermittently. Approximately half way through the experiment, for example, dissolved hydrogen achieved a concentration of 57 mm/kg, which was relatively stable for 700 h, before increasing to approximately 76 mm/kg, which was maintained for the remainder of the experiment (Table 4).

In spite of the high dissolved H_2 and abundant availability of sulfate, only a trace level of dissolved H_2S was observed at approximately 700 h of reaction (Table 4), which decreased subsequently to values below detection. The increasingly high pH may have contributed to this by rendering sulfide minerals insoluble, but it is also likely that sulfate–sulfide equilibrium was not achieved during the experiment, effectively limiting sulfate reduction, precluding significant concentrations of dissolved H_2S. Sulfate–sulfide equilibrium is unlikely in low to moderate temperature subseafloor hydrothermal reactions zones (Ohmoto and Lasaga, 1983; Janecky and Seyfried, 1984).

3.2. Mineral alteration

X-ray diffraction analysis of mineral reaction products following the experiment reveals the abundant presence of serpentine (chrysotile), but also significant amounts of all of the minerals originally making up the peridotite (lherzolite). Anhydrite was also identified by XRD. Petrographic and SEM examination of grain mounts of the reaction products provide additional insight on the fate of the primary minerals in the peridotite following hydrothermal alteration. In particular, these data confirm the presence of all primary minerals, although clinopyroxene coexisting in a matrix of fine-grained serpentine (chrysotile) is particularly noticeable (Fig. 2). Olivine is abundantly present and often associated with brucite (Fig. 2). Cr–spinel and rare Ni–sulfide are also observed in the grain mounts. The lack of magnetite, however, is particularly noteworthy.

The apparent absence of magnetite as indicated by X-ray diffraction data and results of petrographic examination of alteration products motivated the use of other analytical approaches even more sensitive to the presence of this mineral. Accordingly, vibrating sample magnetometer measurements were made on a representative fraction of the bulk alteration products. These data indicate an amount of magnetite no greater than 0.014%, confirming results of the less specific measurements.

Electron microprobe analysis of serpentine reveals compositional homogeneity. Indeed, more than 100 spot measurements of the matrix serpentine failed to indicate any

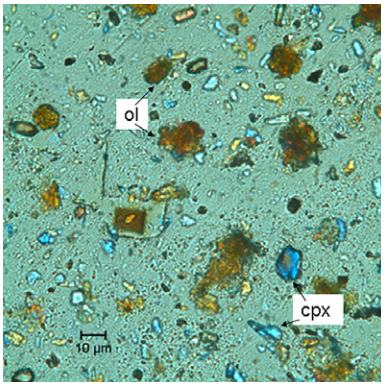

Fig. 2. Petrographic thin section (polished grain mount) of alteration products from the lherzolite–seawater experiment at 200 °C, 500 bar. All of the primary minerals in the peridotite were observed in the alteration products, although clinopyroxene (cpx) (blue under polarized light) appears to be more abundant relative to the starting mineral distribution. Moreover, olivine (ol) tends to be associated with Fe-rich brucite (rusty color), while also abundantly present. All minerals were dispersed in the fine-grained matrix of serpentine. Owing to technical challenges intrinsic to grain mount preparation, however, the observed mineral distribution may not be an entirely accurate representation of the relative abundance of all reaction products. For example, some regions of the slide were associated with spinel and Ni/Fe–sulfide in much greater abundances than possible assuming a representative distribution. (For interpretation of the references to color in this figure legend, the reader is referred to the web version of this paper.)

significant compositional variability (Table 5). Owing to the undetermined presence of structural water (equivalent to approximately 13%) as well as electron channeling between atomic layers and polishing difficulties imposed by the physical properties of the grain mounts, the measured composition failed to achieve 100%. Normalizing the measured composition to a nine-oxygen unit, however, a tri-octahedral structure consistent with serpentine is indicated (Table 5). The measured and calculated serpentine composition indicates significant Fe substitution for Mg, as might be expected considering the likely role of olivine as an alteration precursor. The measured composition of brucite also indicates a general lack of variability, although the lesser number of analyses of this phase makes this more difficult to establish unambiguously. The brucite that was analyzed, however, indicates unusually high Fe (Table 5). Indeed, approximately 30% of the cation occupancy of the octahedral layer is Fe, suggesting the term ferrobrucite might better apply to this particular phase.

Table 5
Electron microprobe analysis of serpentine and brucite produced during the hydrothermal experiment

Component	Serpentine	Brucite
SiO_2	30.24	1.33
TiO_2	0.01	0.00
Al_2O3	0.98	0.65
Cr_2O_3	0.11	0.02
FeO	4.10	32.70
MgO	28.20	38.23
CaO	0.21	0.83
MnO	0.05	1.02
Na_2O	0.09	0.06
K_2O	0.02	0.03
H_2O	nd	nd
Total	64.02	74.87
	Atoms	
	9 (O) Basis	2 (O) Basis
Si	1.95	0.01
Ti	0.01	0.00
Al	0.07	0.01
Cr	0.00	0.00
Cr	0.01	0.00
Fe	0.22	0.30
Mg	2.72	0.63
Ca	0.01	0.01
Mn	0.00	0.00
Na	0.00	0.00
K	0.00	0.00
$(OH)_{calc.}$	4.00	1.00

The reported composition of serpentine represents the average of 100 individual measurements, while that of brucite represents the average of four separate determinations. Compositional variation for both minerals was minor. The relatively low total compositions reported for both minerals, however, represent the lack of determination of structural water and in the case of serpentine, electron channeling between the atomic layers, and polishing difficulties. When normalized to 9 (O, OH), excellent agreement with serpentine is indicated.

4. DISCUSSION

4.1. Serpentinization

Experimental and field investigations of seafloor ultramafic rocks of variable composition have documented the extent and effectiveness of olivine hydrolysis at a wide range of temperatures and pressures (Martin and Fyfe, 1970; Janecky, 1986; Alt and Shanks, 1998; Kelley et al., 2001; Oufi et al., 2002; Allen and Seyfried, 2003; Bach et al., 2004). These data indicate that the hydration and hydrolysis of olivine moves irreversibly in the direction of serpentine minerals, brucite and magnetite at relatively low temperatures and pressures producing $H_{2(aq)}$, as follows:

$$\overset{\text{Olivine(Fo}_{90})}{3Mg_{1.8}Fe_{0.2}SiO_4} + 4.1H_2O \Rightarrow \overset{\text{Serpentine}}{1.5Mg_3Si_2O_5(OH)_4} + \overset{\text{Brucite}}{0.9Mg(OH)_2} + \overset{\text{Magnetite}}{0.2Fe_3O_4} + 0.2H_2 \qquad (2)$$

Obviously for peridotite, the abundance of hydrous alteration phases and time series production of dissolved H_2 would scale with the abundance and rate of olivine and orthopyroxene dissolution, since each contain significant Fe-bearing components (fayalite, ferrosilite). One way to assess mass transfer reactions during peridotite alteration, however, is to conduct a reaction path model taking account of available mineral dissolution rate, composition and abundance data for the primary minerals constituting the peridotite used for the experiment (Tables 1 and 3; Fig. 3). Thus, the experimental data can be used to constrain model predictions.

Model results predict dissolution of more than 90% of the olivine over the course of the approximately 8000-h experiment. The predicted rates of dissolution of orthopyroxene and clinopyroxene (diopside) are considerably less than olivine (Fig. 3a). Indeed, subsequent to a relatively small amount of dissolution during the earliest stages of reaction, diopside is predicted to remain stable thereafter, due to corresponding changes in fluid chemistry (increase in dissolved Ca and pH). The lack of more complete thermodynamic and kinetic data for mineral solid solutions used for the model clearly limits the accuracy of predictions. On the other hand, qualitative insights from these data are generally in keeping with experimental results, although the predicted near total extent of olivine dissolution is clearly at odds with results of the experiment.

In addition to the dissolution of the primary magnesian silicates, model results also show the time-dependent production of secondary phases (Fig. 3b). Not surprisingly, serpentine (chrysotile) is predicted to be the dominant alteration phase followed by brucite, magnetite and then anhydrite. The coexistence of anhydrite with the other alteration phases, as well as residual olivine, is only possible assuming the lack of equilibrium between sulfate and sulfide. That anhydrite was observed by X-ray diffraction of the bulk alteration products, while dissolved sulfate dominated sulfide throughout the experiment is consistent with this assumption. Natural systems likely respond similarly at similar temperatures. For example, vent fluids issuing from the recently discovered Lost City hydrothermal field, offset

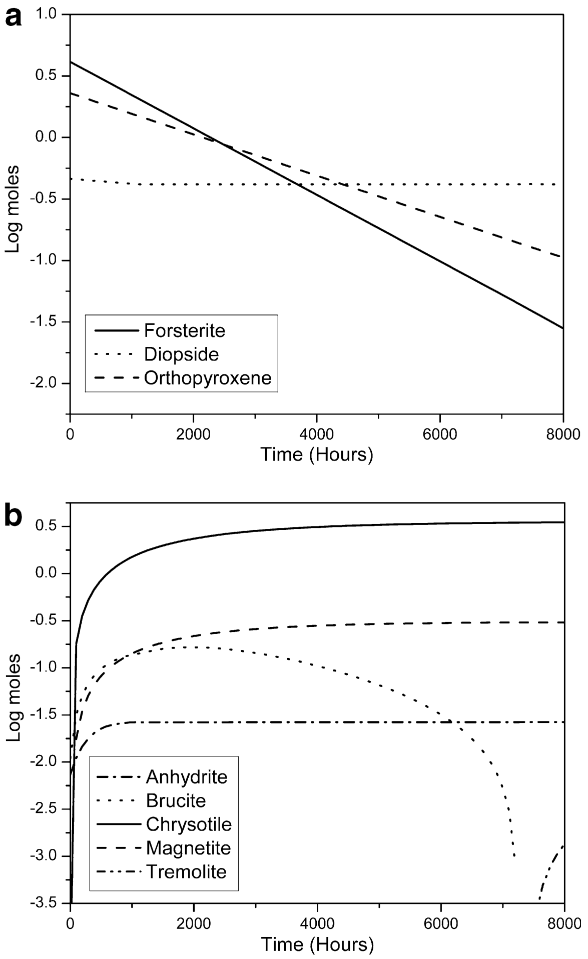

Fig. 3. Calculated lherzolite reaction pathway with seawater as a function of time at a fluid/rock mass ratio of unity at 200 °C, 500 bar. The primary minerals in the lherzolite are predicted to decrease with time in accordance with mineral dissolution rate data (a). Moreover, the opx/forsterite ratio is predicted to increase with reaction progress. The time-dependent change in the relative abundance of primary minerals plays a key role in time series changes in the fluid, which in turn influences the sequence of secondary mineralization (b).

approximately 15 km from the Mid-Atlantic Ridge at 30°N, contain significant dissolved sulfate and dissolved hydrogen, together with low dissolved sulfide (Kelley et al., 2001, 2005; Ludwig et al., 2006), in a manner consistent with model results and experimental data. That subseafloor temperatures at Lost City are likely equivalent to that of the experiment helps to account for this (Allen and Seyfried, 2004).

The predicted formation of hydrous secondary minerals can be expected to cause an increase in dissolved chloride, as observed (Table 4). Thus, comparison between the measured and predicted time series changes in dissolved chloride provides a measure of the relative accuracy of the mineral reaction rate model. Although correspondence exists between the two measures of mineral hydrolysis (Fig. 4), it is clear that by the end of the experiment the measured data are well below the predicted trend. It is important to emphasize that to compare the experimental and theoretical data, it was necessary to correct the predicted trend for the removal of fluid that occurred during sampling. By combining the loss of fluid from sampling effects with mineral hydrolysis rates predicted by the model (Fig. 4), the relatively low measured dissolved chloride suggests that only about 55% of the theoretically possible hydrolysis (olivine, pyroxene) occurred during the experiment, assuming dissolved chloride is a conservative indicator of reaction progress. Thus, the less than expected gain in dissolved chloride indicates lower than expected rates of olivine and pyroxene hydrolysis. This might be caused by uncertainties in the intrinsic rate constants for mineral hydrolysis reactions or armoring of primary mineral reactants by secondary mineral (serpentine, brucite), decreasing effective surface area.

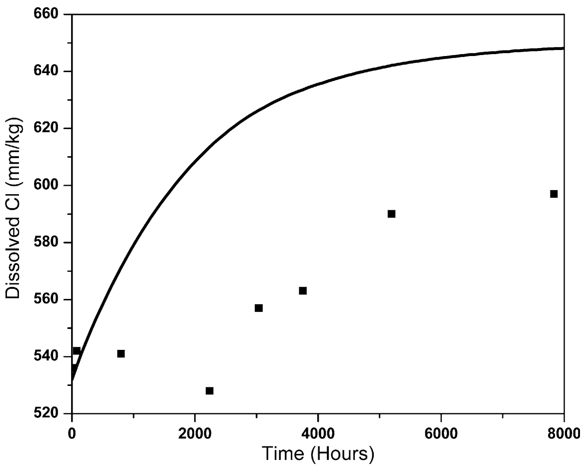

Fig. 4. Predicted (solid line) and measured (solid squares) time series changes in dissolved chloride in fluid coexisting with lherzolite and alteration products at 200 °C, 500 bar and fluid/rock mass ratio of unity. The difference between measured and predicated dissolved Cl concentrations likely reflects differences in the extent of mineral hydrolysis. Thus, the less than expected gain in dissolved chloride indicates lower than expected rates of olivine and pyroxene hydrolysis. Model calculations corrected for sampling (see text) suggest that only about 55% of the theoretically possible hydrolysis (olivine, pyroxene) occurred during the experiment, assuming dissolved chloride is a conservative indicator of reaction progress.

4.2. Phase equilibria effects on pH

The dissolution of olivine and pyroxene solid solutions provide the well known impetus for pH increase in ultramafic-hosted hydrothermal systems, especially at low to moderate temperatures and pressures where these phases are inherently far from equilibrium and dissolve completely given sufficient time (Janecky and Seyfried, 1986; Allen and Seyfried, 2004; Palandri and Reed, 2004). In Mg-bearing seawater, the hydrolysis effects imposed by the dissolution of the primary minerals in ultramafic rocks (e.g., olivine, opx, cpx) are countered by the precipitation of brucite and chrysotile. In chemical systems characterized by relatively low mineral/seawater ratio, as is the case here, seawater-buffering effects are short lived and constraints imposed by the composition of the host rock eventually dominate (Janecky and Seyfried, 1986; Palandri and Reed, 2004).

In general, time series changes in pH and other fluid components measured and predicted from reaction path modeling during the early stages of the experiment are qualitatively in good agreement. The decrease in dissolved Mg and the increase in dissolved Ca are consistent with precipitation of brucite and serpentine and dissolution of diopside, respectively. Mg for Ca exchange associated with this stage of reaction plays a key role in the pH increase (Fig. 5), as emphasized in earlier experimental and theoretical studies of similar compositional systems (Janecky and Seyfried, 1986; Palandri and Reed, 2004). Comparison of experimental data (Table 4 and Fig. 1) with results of the reaction path model subsequent to this very early stage of reaction, however, reveals surprising differences (Fig. 5). For example, in contrast with the theoretically based prediction, the measured dissolved Ca does not maintain a steady state concentration of approximately 30 mm/kg, but rather abruptly decreases after 2200 h of reaction to a value of approximately 7 mm/kg (Table 4 and Fig. 1). Concomitantly, the measured pH ($\mathrm{pH}_{25\,^{\circ}\mathrm{C}}$) increases, ultimately achieving a value of 12.2. Taking account of the effect of temperature on the distribution of aqueous species, the measured pH (25 °C) indicates pH at experimental conditions of 8.7, approximately 0.5 pH units higher than predicted (Fig. 5). In addition to the unexpected decrease in dissolved Ca, the increase in pH subsequent to 2200 h of reaction causes dissolved Mg and SiO_2 to decrease to concentrations below the limits of detection (Table 4 and Fig. 1), again in contrast with theoretical predictions (Fig. 5).

The decrease in dissolved Ca is likely linked to the release of a cation from a component of the mineral reactants that is soluble at experimental conditions, necessitating a corresponding increase in hydroxyl ion to balance charge. The most likely species in this regard is Na, which typically lacks a reversible solubility constraint during hydrothermal alteration in the Na_2O–CaO–MgO–SiO_2–H_2O–HCl system at elevated temperatures and pressures, and is present in an appreciable amount in the clinopyroxene used for the experiment (Table 2). Thus, the incongruent dissolution of the Na_2O component of clinopyroxene may effectively account for the observed abundance of OH^-, as follows:

$$Na_2O(cpx) + H_2O = 2Na^+ + 2OH^- \qquad (3)$$

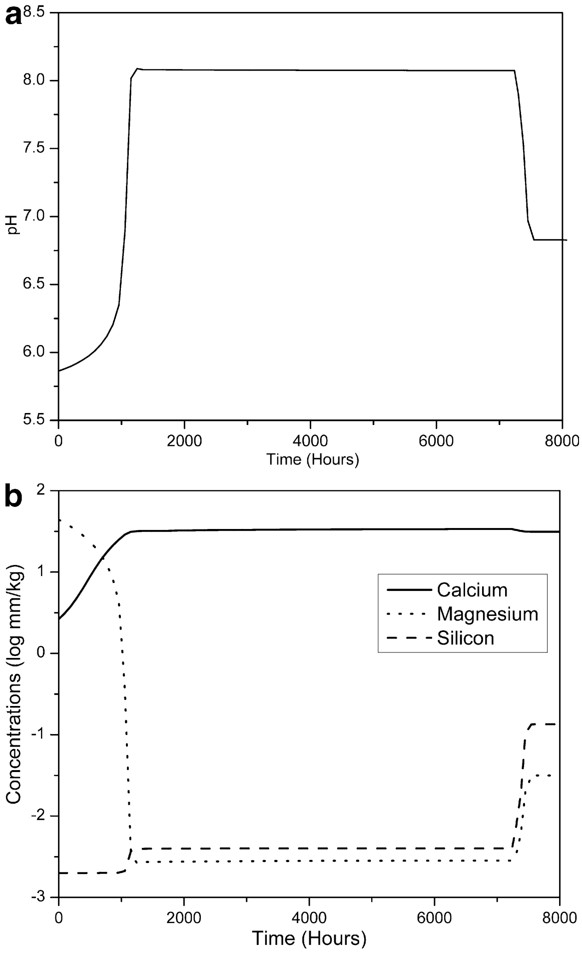

Fig. 5. Calculated time series change in pH (a) (at experimental condition) and (b) dissolved Ca, Mg and Si during reaction pathway model depicting the interaction between seawater and lherzolite at 200 °C, 500 bar and fluid/rock mass ratio of unity. The early to mid-reaction stage pH of approximately 8.2 reflects phase equilibria constraints imposed by chrysotile and brucite. The greater influence of opx dissolution predicted during late stage reaction increases dissolved Si sufficiently to render brucite unstable, resulting in its replacement by chrysotile and tremolite, (see text and Fig. 3). Although the predicted time series changes in fluid chemistry are qualitatively consistent with experimental data, especially during the early sages of reaction, significant departures occur subsequently. The discrepancy in pH with reaction progress is particularly noteworthy, as is the relatively abundant presence of brucite in experimental run products.

Since dissolved chloride increased significantly during the experiment owing to olivine and pyroxene hydrolysis effects, evidence for the Na release mechanism (3) can best be confirmed from time series changes in the Na/Cl ratio. Comparing the Na/Cl ratio to pH with reaction progress (Fig. 6a) provides support for the late stage pH buffering mechanism described above, with concomitant effects on the solubility of Mg and Ca-bearing secondary minerals (Fig. 6b). The pH-induced decrease in dissolved Mg likely results from the precipitation of additional brucite, or formation of clinochlore, especially considering the relative abundance of Al in clinopyroxene (Table 1). Although clinochlore formation can be demonstrated from phase equilibria constraints, it was not identified by X-ray diffraction. The relative abundance of serpentine may have contributed to this. The identity of the Ca-bearing mineral is also not clear, but portlandite is a distinct possibility, in light of the low dissolved silica concentration. Portlandite formation has been proposed for chemical and physical conditions analogous to those of the experiment based on results of theoretical modeling studies (Palandri and Reed, 2004). Similarly, some slab-derived spring waters upwelling through serpentinite mud volcanoes in the Mariana forearc also reveal near quantitative depletions in dissolved Ca,

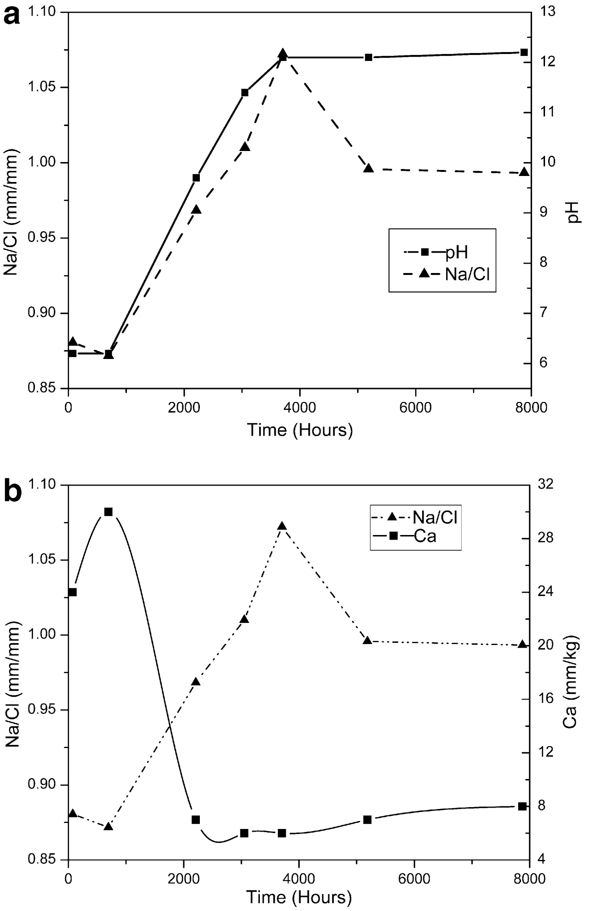

Fig. 6. Experimentally observed correspondence between measured pH (25 °C) and Na/Cl molar ratio during reaction of seawater and lherzolite at 200 °C, 500 bar and fluid/rock mass ratio of unity (a). The increase in chloride normalized dissolved Na likely results from dissolution of a Na_2O component of clinopyroxene (see text), which, in turn, necessitates an increase in hydroxyl ion to balance charge. The high pH causes dissolved Ca to decrease owing to constraints imposed by the solubility of an unidentified Ca-bearing secondary mineral, possible portlandite (b).

high pH and Na/Cl ratios well above seawater (Mottl et al., 2004), suggesting generally similar hydrothermal alteration processes and element exchange patterns. Although the temperatures of the spring waters are relatively low, other chemical and mineralogical data indicate considerably higher temperatures and pressures at the base of the slab from which the fluids are ultimately derived (Maekawa et al., 1993; Fryer et al., 1999; Mottl et al., 2004). In contrast, hydrothermal fluids issuing from the Lost City system do not reveal anomalous Na/Cl ratios or measured pH values in excess of approximately 11. These data suggest phase relations in better agreement with constraints imposed by the compositionally simple theoretical model (Fig. 5) than the more chemically complex assemblage of minerals used for the experimental simulation. Although there may be clinopyroxene in subseafloor hydrothermal reaction zones at Lost City to account for the relatively high dissolved Ca (~30 mm/kg) (Kelley et al., 2005), the chemical components associated with this phase may be sufficiently different from the experiment so as to preclude direct comparisons.

In the absence of a soluble Na-bearing component as existed in the experiment, phase equilibria constraints consistent with the theoretical model (Fig. 5) indicate release of Si during the later stages of the simulation. This is due to the predicted increase in the opx/olivine ratio with reaction progress (Fig. 3). Accordingly, the theoretical data suggest that with time brucite would be "titrated" owing to additions of dissolved silica from opx dissolution, subsequently resulting in tremolite formation (Fig. 3b). Previous experimental, theoretical and field studies have also emphasized this point (Janecky, 1986; Janecky and Seyfried, 1986; Bach et al., 2004). Accordingly, at this stage in the reaction process, pH is predicted to decrease, while dissolved Mg increases slightly (Fig. 5). Even though the pH at conditions (*T*, *P*) is predicted to decrease, the 25 °C equivalent of this is still in excess of 10.5.

4.3. Redox processes

As with high pH conditions, it is well known that hydrothermal alteration processes involving ultramafic rocks at a wide range of temperatures and pressures can result in the generation of unusually reducing conditions (Frost, 1985; Berndt et al., 1996; Allen and Seyfried, 2003, 2004; Sleep et al., 2004; Bach et al., 2006). In general, reducing conditions characterized by high concentrations of dissolved hydrogen result from the oxidation of ferrous silicates by water followed by precipitation of ferric-rich secondary minerals, chiefly magnetite, as illustrated by reaction (2) and Fig. 3b. Results of the mineral dissolution rate model (Fig. 3), however, indicate that over the course of the experiment sufficient time should have been available to permit most of the ferrous iron in olivine to recrystallize to magnetite resulting in a smooth asymptotic increase in dissolved H_2 to a value of approximately 350 mm/kg (Fig. 7). In comparison, the rate of production of dissolved H_2 actually measured reveals a much more complex scenario, characterized by an initially modest rate of increase and then a final concentration that falls below that predicted by approximately a factor of 5 (Fig. 7).

The relatively low production rate of dissolved H_2 during the experiment is consistent with results of field studies of ultramafic-hosted hydrothermal systems that suggest that little magnetite is generated during initial stages of serpentinization, allowing Fe to substitute for Mg in serpentine and brucite, which would then limit the availability of Fe for magnetite, inhibiting large-scale dissolved H_2 production (Toft et al., 1990; Bach et al., 2006). Although such processes may have contributed to mass transfer reactions involving Fe and Mg during the experiment, it fails to account for a key observation, that being the relative absence of magnetite formation *with* H_2 production. Recalling that magnetic susceptibility measurements made on the run products indicate formation of only trace quantities of magnetite (~0.014%), requires that the ferric Fe produced by the oxidation of Fe-bearing components of olivine and orthopyroxene solid solution by H_2O needs to be accommodated largely within the structure of serpentine, the pri-

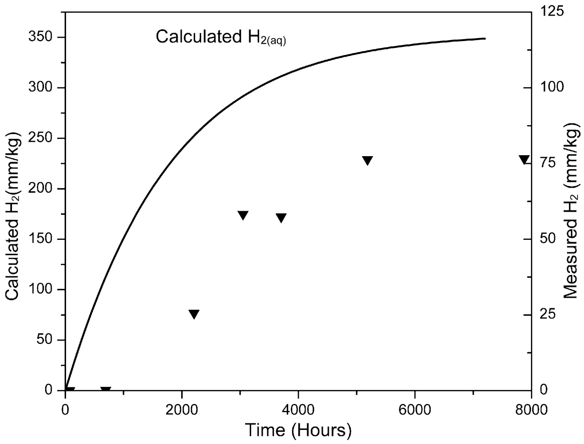

Fig. 7. Calculated (solid line) and measured (solid inverted triangles) time series changes in dissolved hydrogen in fluid coexisting with lherzolite and alteration products. The difference between measured and predicated dissolved H_2 concentrations reflects (in part) the lack of thermodynamic data for Fe-rich secondary minerals in the database used for the theoretical model. The relatively low dissolved H_2 concentration actually measured likely results from: (1) sequestration of ferrous iron in hydrous alteration phases; and, (2) less than anticipated conversion of peridotite minerals to serpentine and brucite during the experiment. Thus, the relatively low dissolved H_2 is consistent with constraints imposed by the relatively low rate of increase in dissolved chloride (see text).

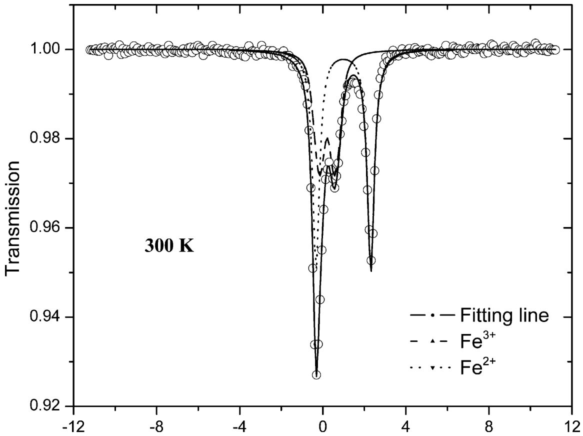

Fig. 8. Mössbauer data for the Fe–serpentine produced during the lherzolite–seawater experiment at 200 °C, 500 bar. The room temperature data (solid line) are comprised of two doublets indicating the presence of both Fe^{+3} (dash line) and Fe^{+2} (dotted line) in the octahedral layer of the serpentine. Modeling results indicate that 58% of the total Fe is ferrous, while the remaining 42% is ferric.

mary alteration mineral. Confirmation of this is provided by Mössbauer spectrometry data, where the spectrum is clearly comprised of two doublets each with a distribution of hyperfine fields indicating the presence of both Fe^{+3} and Fe^{+2} in the octahedral layer of the Fe-rich serpentine (Fig. 8). Moreover, these data indicate that 58% of the total Fe is ferrous, while the remaining 42% is ferric. In the case of Fe-rich brucite, electron microprobe data indicate very significant Fe-enrichment ($X_{Fe} = 0.3$), suggesting a composition approaching that of ferrobrucite.

Thus, the overall reaction that accounts best for the mass transfer of Fe during the experiment is as follows:

$$\begin{aligned} & 4.31\overset{\text{Olivine}}{(Mg_{0.90}Fe_{0.10})_2SiO_4} + 2.64\overset{\text{Orthopyroxene}}{(Mg_{0.87}Fe_{0.13})SiO_3} + 7.99H_2O \\ & \quad = 3.48\overset{\text{Fe–serpentine}}{(Mg_{0.915}Fe^{+2}_{0.04}Fe^{+3}_{0.03})_3Si_2O_5(OH)_4} \\ & \qquad + 0.83\overset{\text{Fe–brucite}}{(Mg_{0.70}Fe_{0.30})(OH)_2} + 0.21H_2. \end{aligned} \tag{4}$$

This reaction assumes complete dissolution of olivine in proportion to that in the lherzolite used for the experiment, but normalized to 1 kg of fluid to facilitate comparison with theoretical models. The reaction further illustrates that the composition and abundance of hydrous alteration minerals requires alteration of virtually all-available orthopyroxene. Owing to the formation of the ferric component of serpentine, however, reaction (4) indicates the capacity to generate 210 mm/kg dissolved H_2, well below that predicted assuming complete reaction of the lherzolite, while *ignoring Fe-uptake by secondary silicates* (Fig. 7), underscoring the significance of Fe sequestration in minerals on the rate and magnitude of production of dissolved H_2. This, however, is not sufficient to explain the times series data for dissolved H_2 observed during the experiment, in which even after nearly 8000 h of reaction, less than 77 mm/kg dissolved H_2 is produced (Table 4), far below the 210 mm/kg indicated by reaction (4).

The relatively low dissolved H_2 measured during the experiment provides supporting data for the previous interpretation based on the time series increase of dissolved chloride that a less than complete reaction occurred, the relatively long reaction time notwithstanding. Indeed, the two indicators of reaction progress are in reasonably close agreement with the chloride and H_2 data suggesting factors of approximately 2 and 3, respectively, between the hydrolysis theoretically possible (100% reaction) and that which was actually observed. The differences between the two estimates are likely related to model dependencies. In the case of dissolved H_2, it is possible that Fe-bearing alteration products other than depicted by reaction (4) exist, but were simply not observed by XRD and petrographic studies. For example, high-resolution TEM results of aqueous alteration studies of the olivine (Fe-rich) bearing Allende meteorite at temperature, pressure and fluid/rock mass ratios analogous to the present study indicate the formation of a range of unusually fine grained (submicron) Fe-bearing minerals along olivine grain boundaries (Jones and Brearley, 2006). In one experiment at 200 °C and fluid/rock mass ratio of 9, these investigators reported individual phyllosilicate crystals that reach 30 units cells wide (~100 nm) and form anastomosing networks over the surface of olivine reactants. In addition to retaining Fe, mineralization such as this may eventually limit access of fluid to olivine producing a negative feedback mechanism that ultimately would decrease rates of alteration of olivine and that of other primary silicates so affected. The alteration minerals observed in the Allende study include serpentine and saponite that contain both ferric and ferrous iron. Thus, it is clear, that for theoretical models to predict accurately rates and processes of mass transfer involving Fe in ultramafic-hosted hydrothermal systems, Fe-enrichment in secondary phases involving both ferric and ferrous components needs to be considered on potentially very fine scales.

4.3.1. Stability of Fe-bearing serpentine and brucite with implications for mass transfer during serpentinization

The Fe-bearing serpentine that formed by the end of the peridotite experiment at 200 °C, 500 bar can be depicted as follows:

$$\overset{Fe^{+2,+3}\text{–bearing serpentine}}{(Mg_{0.915}Fe^{+2}_{0.04}Fe^{+3}_{0.03})_3Si_2O_5(OH)_4} + 0.255\overset{\text{Brucite}}{Mg(OH)_2} = \overset{\text{Chrysotile}}{Mg_3Si_2O_5(OH)_4} + 0.07\overset{\text{Magnetite}}{Fe_3O_4} + 0.025\,H_2 + 0.23\,H_2O \tag{5}$$

where, the composition of the serpentine is that determined from electron microprobe analysis, while the distribution of Fe between ferric and ferrous components is based on the Mössbauer data (Fig. 8). Brucite and chrysotile solid solutions are the primary alteration mineral candidates for the system. Although magnetite was not identified by petrographic examination of reaction products, the presence of trace magnetite was confirmed by susceptibility measurements, as described previously. Standard state conventions are unit activity at temperature and pressure for stoichiometric minerals and water and unit activity of a hypothetical one molal solution at infinite dilution. We assume unit activities for the Fe-bearing serpentine, magnetite, and water, while activities of other solid phases were computed assuming ideal site mixing (i.e., $a_{\text{Mg–chrysotile}} = X^3_{\text{Mg–chrysotile}}$ and $a_{\text{Mg–brucite}} = X_{\text{Mg–brucite}}$) (Table 5). Thus, taking account of activity–composition relations as described along with the measured dissolved H_2 (76.7 mm/kg) a value of −0.027 can be determined for the equilibrium constant ($\log K$) for reaction (5) (Table 6). It is important to emphasize that this value is provisional, since efforts were not made towards the end of the experiment to reverse the dissolved H_2 concentration. This point notwithstanding, the measured H_2 is in good agreement with that estimated for fluids coexisting with Fe–serpentine and Fe–brucite at 200 °C, when the mole fraction of Fe^{+2} in serpentine is analogous to that observed for the present experiment (Sleep et al., 2004). The ratio of the experimentally observed mole fraction of Fe^{+2} in brucite to that in serpentine, however, is considerably greater (~7.5) than the value of 2 estimated by Sleep et al. (2004), which is based on coexisting compositions of brucite and lizardite in serpentinites reported in the literature (Evans and Trommsdorf, 1972). More recently, Bach et al. (2006) also determined the chemical and mineralogical composition of serpentinites recovered from MAR 15°N (ODP Leg 209, Site 1274). These investigators noted that during late stage serpentinization characterized by the flux of relatively large amounts of fluid under decidedly open system conditions, the ratio of the mole fraction of Fe in brucite to that in serpentine is also approximately 2.

The study by Bach et al. (2006) documented that magnetite formation is largely restricted to the latter stages of the serpentinization process when presumably lower pH and more oxidizing conditions prevail, contributing to the dissolution of Fe-rich serpentine and brucite. The fluid-dominated conditions that occur would effectively preclude redox and pH buffering by primary minerals in peridotite, enhancing magnetite formation. The closed-system conditions that inherently characterize the present study inhibit quantitative dissolution of olivine and orthopyroxene, resulting in high-pH, reducing conditions more favorable to the incorporation of Fe in serpentine and brucite rather than magnetite, perhaps helping to explain the relatively high X_{Fe} for brucite in comparison with results from field studies. A secondary factor contributing to the lack of magnetite formation during the present study, however, may involve mineral reaction kinetics. Accordingly, the rates of formation of serpentine and brucite at the chemical and physical conditions that prevailed during the experiment may have been sufficiently favorable that Fe was unavailable for other minerals. Thus, the experimental results likely simulate the earliest stages of natural systems undergoing serpentinization. Although it is commonly accepted that the flux of H_2 is limited by the lack of magnetite formation during this stage of alteration (Bach et al., 2006), the results of the present study indicate that this need not be the case owing to the formation of a ferric component of serpentine.

Expressing reaction (5) ($Fe^{+2,+3}$-bearing serpentine) in terms of aqueous basis species (Table 6), while doing the same for Fe-bearing brucite (following conversion from mole fraction Fe ($X_{Fe=0.3}$) to activity using the ideal site mixing model discussed earlier), permits incorporation of mineral hydrolysis constants for these minerals into reac-

Table 6
Hydrolysis constant for $Fe^{+2,+3}$-bearing serpentine generated during the lherzolite–seawater experiment at 200 °C, 500 bar

Reaction	Log *K*
$\overset{Fe^{+2,+3}\text{–serpentine}}{(Mg_{0.915}Fe^{+2}_{0.04}Fe^{+3}_{0.03})_3Si_2O_5(OH)_4} + 0.255\overset{\text{Brucite}}{Mg(OH)_2} = \overset{\text{Chrysotile}}{Mg_3Si_2O_5(OH)_4} + 0.07\overset{\text{Magnetite}}{Fe_3O_4} + 0.025H_2 + 0.23H_2O$	−0.0270
$Mg_3Si_2O_5\,(OH)_4 + 6H^+ = 2\ SiO_2 + 3Mg^{+2} + 5H_2O$	16.9230
$0.07 * (Fe_3O_4 + 8H^+ = Fe^{+2} + 2\ Fe^{+3} + 4H_2O)$	−3.2260
$0.255 * (Mg^{+2} + 2H_2O = Mg(OH)_2 + 2\ H^+)$	−9.4170
$0.05 * (Fe^{+3} + 0.5H_2 = Fe^{+2} + H^+)$	11.7735
$(Mg_{0.915}Fe^{+2}_{0.04}Fe^{+3}_{0.03})_3Si_2O_5(OH)_4 + 6H^+ = 2.745Mg^{+2} + 0.12Fe^{+2} + 0.09Fe^{+3} + 2SiO_2 + 5H_2O$	14.8575

Supporting thermodynamic data for minerals and aqueous species are from SUPCRT92 (Johnson et al., 1992) (see text).

tion path computer modeling software, such as EQ3/6 (Wolery and Daveler, 1992) and GWB (Bethke, 1994). Accordingly, assessment of the effects of $Fe^{+2,+3}$-bearing serpentine and Fe–brucite on hydrothermal alteration processes in systems undergoing serpentinization can be predicted, against which field observations can be compared. Although there are a number of different approaches that can be taken to accomplish this, we chose to use a simple kinetic model in which unreacted fluid (seawater) incrementally enters the system while displacing an equal volume of reacted fluid, simulating better a natural open-system. Reaction progress is not a measure of time, but rather an indicator of the number of kilograms of seawater added to the system following equilibration during each increment.

The earlier stage of reaction depicted in the simulation is analogous to full equilibrium at a fluid (seawater)–lherzolite ratio of unity (Fig. 9). Thus, the abundance of $Fe^{+2,+3}$-bearing serpentine and Fe–brucite is not surprising, especially in light of the procedures used to regress the stability of the serpentine. The incremental addition of seawater enhances Mg–Fe exchange and Mg–Ca exchange resulting in increases in pure Mg–chrysotile and anhydrite and the dissolution of Fe–serpentine, Fe–brucite and diopside. Sulfate–sulfide equilibrium was not considered during the simulation, for reasons discussed previously (Ohmoto and Lasaga, 1983; Janecky and Seyfried, 1986).

The dissolution of Fe-bearing serpentine and brucite is also accompanied by an increase in magnetite, which completely replaces the former assemblage of minerals mid-way through the simulation (Fig. 9). The database used for the model contained Fe-bearing secondary phases directly analogous to those observed in the experiment, and thus, precluded systematic changes in the composition of these minerals with reaction progress. In natural systems, however, it is likely that the dissolution of both Fe–serpentine and Fe–brucite might be more gradual as these phases become increasingly Mg-rich, perhaps ultimately resulting in the ratio of X_{Fe} in brucite to serpentine of 2, consistent with field observations. In any event, it is unlikely that the Fe-bearing assemblages (serpentine, brucite) would endure beyond that predicted for pure brucite, since at this point reaction progress conditions are becoming sufficiently oxidizing that Fe-enrichment in minerals other than magnetite and ultimately hematite is unlikely.

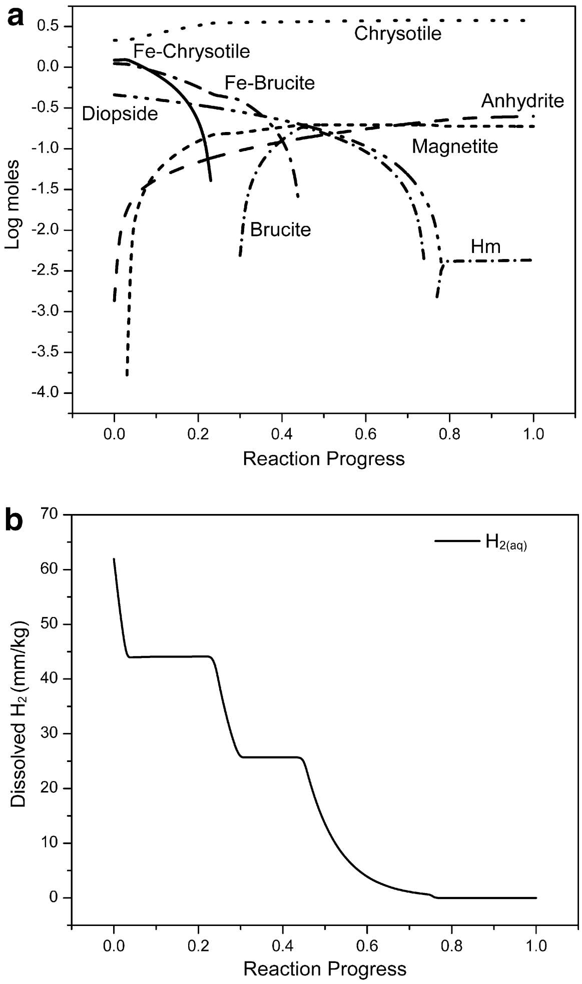

Fig. 9. Calculated reaction path model depicting the incremental addition of seawater into a lherzolite-bearing reaction zone at 200 °C, 500 bar. Provisional thermodynamic data for Fe–serpentine and Fe–brucite from experimental results have been added to the model database as described in the text. Each 0.1 unit of reaction progress reflects addition and displacement of 1 kg seawater, simulating in part an open geochemical system. Full equilibrium is achieved at each incremental stage of reaction. The model predicts the relative abundance of Fe-bearing secondary minerals at low fluid/rock mass ratios, with the dissolution of these phases with addition of incrementally greater amounts of seawater (a). A stepwise decrease in dissolved H_2 with reaction progress reflects the systematic change in redox buffer capacity with changes in mineralization (b). Sulfate–sulfide equilibrium was suppressed (see text).

Chemical and mineralogical change induced by the incremental addition of seawater into a peridotite-bearing reaction zone is likely dominated by changes in dissolved H_2, which is predicted to decrease with reaction progress (Fig. 9b). The predicted decrease, however, is not gradual as might be the case for a conservative component undergoing dilution, but rather is revealed by a series of steps, reflecting corresponding changes to redox-buffering mineral assemblages. The first step is encountered immediately and likely represents the redox buffer capacity induced by the coexistence of Fe–serpentine and Fe–brucite. The second redox step correlates with the increasing formation of magnetite, resulting in a magnetite–Fe–brucite buffer, while the asymptotic decrease in dissolved H_2 that is predicted to occur with further reaction progress correlates in the extreme with the coexistence of magnetite and hematite. Although it is often suggested that serpentinization reactions are inherently reducing, the results of model calculations indicate that sharp redox gradients are likely dependent on the stage of reaction, with the end stages in open systems being the least reducing. Evidence from natural serpentinites of a magnetite-dominated stage of reaction is in and of itself not indicative of unusually reducing conditions, especially considering the capacity of ferric-iron enrichment in serpentine to generate H_2 in the absence of magnetite and the buffering (dilution) effects imposed by the circulation of seawater during later stages of alteration when magnetite formation is more likely.

The earliest stages of serpentinization can indeed be distinctly reducing, especially if mass transfer reactions involving olivine and pyroxene hydrolysis have time to progress sufficiently to form abundant ferric-rich serpentine (reaction 5). Accordingly, the corresponding release of dissolved H_2 could play a key role in reactions involving hydrocarbon synthesis as well as in microbial metabolism distal to the primary site of formation of the H_2-bearing fluids. For example, endmember hydrothermal vent fluids issuing from carbonate and brucite-bearing chimney structures at the ultramafic-hosted Lost City hydrothermal field not only reveal significant concentrations of dissolved H_2 (~15 mm/kg), but also dissolved CH_4 (~2 mm/kg) (Kelley et al., 2005), and likely other dissolved hydrocarbons as well. Although the origin of methane in these and other subseafloor hydrothermal fluids is complex and still not completely understood, one interpretation involves mineral catalyzed carbon reduction that are driven by the coexisting concentrations of dissolved H_2 and CO_2 and linked to methane by a Fischer–Tropsch type mechanism (Horita and Berndt, 1999; McCollom and Seewald, 2001; Foustoukos and Seyfried, 2004; Fu et al., 2007):

$$CO_2 + 4H_2 = CH_4 + 2H_2O. \quad (6)$$

In many geologic systems, however, chemical and physical conditions work against methane formation at rates sufficient to enhance formation of thermodynamically less stable carbon compounds (Seewald et al., 2006). The formation of such species has important implications for all mass transfer reactions involving aqueous carbon in subseafloor hydrothermal systems, including those that are microbially mediated at vents. While kinetic barriers inhibiting methane formation are an essential prerequisite for synthesis of complex hydrocarbons, a more fundamental constraint involves the existence of highly reducing conditions that are largely governed by meta-stability in the $FeO–Fe_2O_3–MgO–SiO_2–H_2O$ system of the type recognized during the present investigation.

5. SUMMARY

Results of an experiment involving peridotite (lherzolite) and seawater reacted in equal proportions at 200 °C, 500 bar reveal complex times series changes in fluid chemistry that place key constraints on the mechanism of alteration and rates of mass transfer processes in ultramafic-hosted hydrothermal systems. Mg for Ca exchange occurred relatively rapidly, and was complete by approximately 700 h. In response to the gain in dissolved Ca, dissolved sulfate decreased, due to precipitation of anhydrite. Surprisingly, dissolved Ca did not maintain its concentration maximum (30 mm/kg) at 700 h, but decreased subsequently, while dissolved sulfate increased owing to constraints imposed by anhydrite solubility. The decrease in dissolved Ca correlates with an increase in Na/Cl ratio, likely linked to the dissolution of the Na_2O component in clinopyroxene, one of the primary minerals constituting lherzolite. Concomitantly, the measured pH (25 °C) increased dramatically, even above already high values. The observed changes in pH throughout the experiment can be linked to constraints imposed by the solubility of Mg, Ca and finally Na-bearing phases, the latter being responsible for the build up in Na^+ and OH^-, to balance charge. Dissolved chloride and K generally increased in response to mineral hydration and hydrolysis, while dissolved silica, Fe and H_2S decreased due to solubility control in the increasingly high pH fluids. Dissolved H_2 increased at irregular intervals, finally achieving a value of approximately 77 mm/kg at the end of the nearly 8000-h experiment. The relatively long reaction time notwithstanding, all of the primary minerals in the peridotite were observed along with secondary serpentine and brucite.

Taking explicit account of available mineral dissolution rate data, predictions of time series changes in solution were compared with experimental observations. Modeling results indicate rates of mineral dissolution as follows: olivine $>$ orthopyroxene $\gg$ clinopyroxene (diopside). Moreover, dissolved chloride is predicted to increase, but exceeds that measured by approximately 40% when sampling effects are explicitly accounted for. The cause of this may be related to uncertainties in the rate data and/or changes in the surface area of mineral reactants induced by precipitation of secondary minerals. The formation of magnetite in particular is predicted to release relatively large quantities of dissolved H_2, in great excess of the concentrations actually observed.

The differences between experimental and theoretical data are caused almost entirely by inconsistencies in the composition and abundance of alteration minerals. Although most of the minerals predicted to form were actually observed following the experiment, the experimentally derived chrysotile and brucite contain abundant Fe. Moreover, Mössbauer data indicate that approximately 50% of the Fe in serpentine is ferric, which agrees well with the observed increase in dissolved H_2 in the relative absence of significant formation of magnetite. The relatively minor formation of magnetite during the experiment was confirmed by magnetic susceptibility measurements. As with changes in dissolved chloride, time series changes in dissolved H_2 observed during the experiment reflect rates of mass transfer less than theoretically possible. Thus, model results, which provide useful qualitative data on serpentinization processes, are not quantitatively accurate owing to the inherent lack of kinetic and thermodynamic data for Fe-bearing alteration phases, especially serpentine, which contains both ferric and ferrous components.

Measured dissolved H_2 coexisting with Fe bearing serpentine and brucite permits calculation of provisional thermodynamic data for these phases, which can be combined with existing thermodynamic data to better assess the effects of fluid–rock interaction in natural systems undergoing serpentinization. In a manner consistent with field observations, model results indicate late-stage formation of magnetite following circulation of sufficient fluid (seawater) to render Fe-bearing serpentine and brucite unstable. Even in the absence of magnetite formation, the earliest stages of reaction can release very significant amounts of dissolved H_2, which could play a key role in organic syntheses and microbial metabolism in ultramafic-hosted hydrothermal systems.

ACKNOWLEDGMENTS

We thank Mr. Rick Knurr, Department of Geology and Geophysics at the University of Minnesota, for development of new analytical approaches without which the study could not have been conducted. We also thank Ms. Miki Rough (McGill University) for her assistance with petrographic analysis of experimental run products, and Dr. Bruce Moskowitz, Department of Geology and Geophysics, University of Minnesota, who provided magnetic intensity measurements and Mössbauer data of serpentine alteration minerals. Helpful comments by Associate Editor Jeff Alt, J.L. Charlou, Mike Mottl, D.E. Allen, and one anonymous reviewer are greatly appreciated. This work was made possible with financial support provided through NSF Grant OCE-054957.

REFERENCES

Aagaard P. and Helgeson H. C. (1982) Thermodynamic and kinetic constraints on reaction rates among minerals and aqueous solutions. I. Theoretical considerations. *Amer. J. Sci.* **282**, 237–285.

Allen D. E. and Seyfried, Jr., W. E. (2003) Alteration and mass transfer in the MgO–CaO–FeO–Fe_2O_3–SiO_2–Na_2O–H_2O–HCl system at 400 °C and 500 bars: implications for pH and compositional controls on vent fluids from ultramafic-hosted hydrothermal systems at mid-ocean ridges. *Geochim. Cosmochim. Acta* **67**, 1531–1542.

Allen D. E. and Seyfried, Jr., W. E. (2004) Serpentinization and heat generation: constraints from Lost City and Rainbow hydrothermal systems. *Geochim. Cosmochim. Acta* **68**(6), 1347–1355.

Alt J. C. and Shanks, III, W. C. (1998) Sulfur in serpentinized oceanic peridotite: serpentinization processes and microbial sulfate reduction. *J. Geophys. Res.* **103**(5), 9917–9929.

Bach W., Garrido C. J., Paulick H., Harvey J. and Rosner M. (2004) Seawater–peridotite interactions: first insights from ODP Leg 209, MAR 15°N. *Geochem. Geophys. Geosys.* **5**. doi:10.1029/2004GC00074.

Bach W., Paulick H., Garrido C. J., Ildefonse B., Meurer W. P. and Humphris S. E. (2006) Unraveling the sequence of serpentinization reactions: petrography, mineral chemistry, and petrophysics of serpentinites from MAR 15°N (ODP Leg 209, Site 1274). *Geophys. Res. Lett.* **33**(L13306). doi:10.1029/2006GL02568.

Berndt M. E., Allen D. E. and Seyfried, Jr., W. E. (1996) Reduction of CO_2 during serpentinization of olivine at 300 °C and 500 bars. *Geology* **24**(4), 351–354.

Bethke, C. M. (1994) *The Geochemist's WorkbenchTM, version 2.0. A User's Guide to Rxn, Act2, React, and Gtplot*. Hydrogeology Program, University of Illinois.

Cannat M. (1993) Emplacement of mantle rocks in the seafloor at mid-ocean ridges. *J. Geophys. Res.* **98**, 4163–4172.

Cannat M., Bideau D. and Bougault H. (1992) Serpentinized peridotites and gabbros in the Mid-Atlantic Ridge axial valley at 15°37′N and 16°52′N. *Earth Planet. Sci. Lett.* **109**(1–2), 87–106.

Escartin J. and Cannat M. (1999) Ultramafic exposures and the gravity signature of the lithosphere near the Fifteen–Twenty Fracture Zone (Mid-Atlantic Ridge, 14°–16.5°N). *Earth Planet. Sci. Lett.* **171**(3), 411–424.

Escartin J., Hirth G. and Evans B. (1997) Effects of serpentinization on the lithospheric strength and the style of normal faulting at slow-spreading ridges. *Earth Planet. Sci. Lett.* **151**(3–4), 181–189.

Evans B. W. and Trommsdorf V. (1972). *Der Einfluss des Eisen auf die Hydratisierung on Duniten Schweizerische Mineralogische und Petrographische Mitteilungen* **52**, 251–256.

Foustoukos D. I. and Seyfried, Jr., W. E. (2004) Hydrocarbons in hydrothermal vent fluids: the role of chromium-bearing catalysts. *Science* **304**(5673), 1002–1005.

Foustoukos D. I. and Seyfried, Jr., W. E. (2005) Redox and pH constraints in the subseafloor root zone of the TAG hydrothermal system, 26 °N Mid-Atlantic Ridge. *Earth Planet. Sci. Lett.* **235**(3–4), 497–510.

Frost B. R. (1985) On the stability of sulfides, oxides and native metals in serpentinites. *J. Petrol.* **26**, 31–63.

Fryer P., Wheat C. G. and Mottl M. J. (1999) Mariana blueschist mud volcanism: implications for conditions within the subduction zone. *Geology* **27**(2), 103–106.

Fu Q., Sherwood Lollar B., Horita J., Lacrampe-Couloume G. and Seyfried, Jr., W. E. (2007) Abiotic formation of hydrocarbons under hydrothermal conditions: constraints from chemical and isotope data. *Geochim. Cosmochim. Acta* **71**(8), 1982–1998.

Helgeson H. C., Murphy W. M. and Aagaard P. (1984) Thermodynamic and kinetic constraints on the reaction rates among minerals and aqueous solutions: II. Rate constants, effective surface area, and the hydrolysis of feldspar. *Geochim. Cosmochim. Acta* **48**(12), 2405–2433.

Horita J. and Berndt M. E. (1999) Abiogenic methane formation and isotopic fractionation under hydrothermal conditions. *Science* **285**(5430), 1055–1057.

Janecky, D. R. (1986) *Serpentinization Reaction Pathways: Implications for Modeling Approach*. Proceedings of the Workshop on Geochemical Modeling (LLNL CONF-8609134).

Janecky D. R. and Seyfried, Jr., W. E. (1984) Formation of massive sulfide deposits on oceanic ridge crests: incremental reaction models for mixing between hydrothermal solutions and seawater. *Geochim. Cosmochim. Acta* **48**, 2723–2738.

Janecky D. R. and Seyfried W. E. (1986) Hydrothermal serpentinization of peridotite within the oceanic crust: experimental investigations of mineralogy and major element chemistry. *Geochim. Cosmochim. Acta* **50**, 1357–1378.

Johnson J. W., Oelkers E. H. and Helgeson H. C. (1992) SUPCRT92—a software package for calculating the standard molal thermodynamic properties of minerals, gases, aqueous species, and reactions from 1-bar to 5000-bar and 0 °C to 1000 °C. *Comput. Geosci.* **18**(7), 899–947.

Jones C. L. and Brearley A. J. (2006) Experimental aqueous alteration of the Allende meteorite under oxidizing conditions: constraints on asteroidal alteration. *Geochim. Cosmochim. Acta* **70**, 1040–1068.

Kelley D. S., Karson J. A., Blackman D. K., Fruh-Green G. L., Butterfield D. A., Lilley M. D., Olson E. J., Schrenk M. O., Roe K. K., Lebon G. T. and Rivizzigno P. (2001) An off-axis hydrothermal vent field near the Mid-Atlantic Ridge at 30°N. *Nature* **412**(6843), 145–149.

Kelley D. S., Karson J. A., Fruh-Green G. L., Yoerger D. R., Shank T. M., Butterfield D. A., Hayes J. M., Schrenk M. O., Olson E. J., Proskurowski G., Jakuba M., Bradley A., Larson B., Ludwig K., Glickson D., Buckman K., Bradley A. S., Brazelton W. J., Roe K., Elend M. J., Delacour A., Bernasconi S. M., Lilley M. D., Baross J. A., Summons R. E. and Sylva S. P. (2005) A serpentinite-hosted ecosystem: the Lost City hydrothermal field. *Science* **307**(5714), 1428–1434.

Knauss K. G., Nguyen S. N. and Weed H. C. (1993) Diopside dissolution kinetics as a function of pH, CO_2, temperature, and time. *Geochim. Cosmochim. Acta* **57**(2), 285–294.

Lasaga, A. C. (1981) Transition state theory. In *Kinetics of Geochemical Processes*, vol. 8 (eds. A. C. Lasaga and R. J. Kirkpatrick), pp. 135–169.

Ludwig K. A., Kelley D. S., Butterfield D. A., Nelson B. K. and Fruh-Green G. (2006) Formation and evolution of carbonate chimneys at the Lost City hydrothermal field. *Geochim. Cosmochim. Acta* **70**(14), 3625–3645.

Maekawa H., Shozul M., Ishii T., Fryer P. and Pearce J. A. (1993) Blueschist metamorphism in an active subduction zone. *Nature* **364**(6437), 520–523.

Martin B. and Fyfe W. S. (1970) Some experimental and theoretical observations on the kinetics of hydration reactions with particular reference to serpentinization. *Chem. Geol.* **6**, 185–202.

McCollom T. M. and Seewald J. S. (2001) A reassessment of the potential for reduction of dissolved CO_2 to hydrocarbons during serpentinization of olivine. *Geochim. Cosmochim. Acta* **65**, 3769–3778.

Mottl M. J., Wheat C. G., Fryer P., Gharib J. and Martin J. B. (2004) Chemistry of springs across the Mariana forearc shows progressive devolatilization of the subducting plate. *Geochim. Cosmochim. Acta* **68**(23), 4915–4933.

Murphy W. M. and Helgeson H. C. (1987) Thermodynamic and kinetic constraints on reaction rates among minerals and aqueous solutions. III. Activated complexes and the pH-dependence of the rates of feldspar, pyroxene, wollastonite, and olivine hydrolysis. *Geochim. Cosmochim. Acta* **51**(12), 3137–3153.

Nagy, K. L. (1995) Dissolution and precipitation kinetics of sheet silicates. In *Chemical Weathering Rates of Silicate Minerals*, vol. 31 (eds. A. F. White and S. L. Brantley). Mineralogical Society of America, Washington, DC, pp. 173–233.

Ohmoto H. and Lasaga A. C. (1983) Kinetics of reactions between aqueous sulfates and sulfides in hydrothermal systems. *Geochim. Cosmochim. Acta* **46**, 1727–1746.

Oufi O., Cannat M. and Horen H. (2002) Magnetic properties of variably serpentinized abyssal peridotites. *J. Geophys. Res.* **107**(B5), 2095–2113.

Palandri J. L. and Reed M. H. (2004) Geochemical models of metasomatism in ultramafic systems: serpentinization, rodingitization, and sea floor carbonate chimney precipitation. *Geochim. Cosmochim. Acta* **68**(5), 1115–1133.

Pokrovsky O. S. and Schott J. (2000) Kinetics and mechanism of forsterite dissolution at 25 °C and pH from 1 to 12. *Geochim. Cosmochim. Acta* **64**, 3313–3325.

Schott J., Berner R. A. and Sjoberg E. L. (1981) Mechanism of pyroxene and amphibole weathering. I. experimental studies of iron-free minerals. *Geochim. Cosmochim. Acta* **45**, 2123–2138.

Schrenk M. O., Kelley D. S., Bolton S. A. and Baross J. A. (2004) Low archaeal diversity linked to subseafloor geochemical processes at the Lost City Hydrothermal Field, mid-Atlantic ridge. *Environ. Microbiol.* **6**(10), 1086–1095.

Seewald J. S., Zolotov M. Y. and McCollom T. (2006) Experimental investigation of single carbon compounds under hydrothermal conditions. *Geochim. Cosmochim. Acta* **70**(2), 446–460.

Seyfried, Jr., W. E. and Dibble, Jr., W. E. (1980) Seawater–peridotite interaction at 300 degrees C and 500 bars; implications for the origin of oceanic serpentinites. *Geochim. Cosmochim. Acta* **44**(2), 309–322.

Seyfried, Jr., W. E., Janecky D. R. and Berndt M. E. (1987) Rocking autoclaves for hydrothermal experiments. II. The flexible reaction-cell system. In *Hydrothermal Experimental Techniques* (eds. G.C. Ulmer and H.L. Barnes). Wiley-Intescience, pp. 216–239.

Shock E. L. and Helgeson H. C. (1988) Calculation of the thermodynamic and transport properties of aqueous species at high pressures and temperatures: correlation algorithms for ionic species and equation of state predictions to 5 kb and 1000 °C. *Geochim. Cosmochim. Acta* **52**, 2009–2036.

Shock E. L. and Helgeson H. C. (1990) Calculation of the thermodynamic and transport properties of aqueous species at high pressures and temperatures: standard partial molal properties of organic species. *Geochim. Cosmochim. Acta* **54**, 915–945.

Shock E. L., Sassani D. C., Willis M. and Sverjensky D. A. (1997) Inorganic species in geologic fluids: correlations among standard molal thermodynamic properties of aqueous ions and hydroxide complexes. *Geochim. Cosmochim. Acta* **61**, 907–950.

Sleep N. H., Meibom A., Fridriksson T., Coleman R. G. and Bird D. K. (2004) H2-rich fluids from serpentinization: geochemical and biotic implications. *Proc. Natl. Acad. Sci. USA* **101**(35), 12818–12823.

Snow J. E. and Dick H. J. (1995) Pervasive magnesium loss by marine weathering of peridotite. *Geochim. Cosmochim. Acta* **59**, 4219–4235.

Sverjensky D. A., Shock E. L. and Helgeson H. C. (1997) Prediction of the thermodynamic properties of aqueous metal complexes to 1000 °C and 5 kb. *Geochim. Cosmochim. Acta* **61**(7), 1359–1412.

Tanger J. C. and Helgeson H. C. (1988) Calculation of the thermodynamic properties of aqueous species at high pressure and temperatures: revised equation of state for the standard partial properties of ions and electrolytes. *Amer. J. Sci.* **288**, 19–98.

Toft P. B., Arkani-Hamed J. and Haggerty S. E. (1990) The effects of serpentinization on density and magnetic susceptibility: a petrophysical model. *Phys. Earth Planet. Int.* **65**, 137–157.

Wolery, T. J. and Daveler, S. A. (1992) *EQ6, A Computer Program for Reaction Path Modeling of Aqueous Geochemical Systems: Theoretical Manual, Users Guide, and Related Documentation (version 7.0)*. UCRL-MA-110662, PT IV, pp. 1–337.

Zimmerman M. E. and Kohlstedt D. L. (2004) Rheological properties of partially molten lherzolite. *J. Petrol.* **45**(2), 275–298.

Associate editor: Jeffrey C. Alt